

Article

Impact of Zinc Oxide on the Structure and Surface Properties of Magnesium–Potassium Glass–Crystalline Glazes

Katarzyna Pasiut , Janusz Partyka , Dawid Kozień  and Piotr Pańtak 

Department of Ceramics and Refractory Materials, Faculty of Materials Science and Technology, AGH University of Science and Technology, Mickiewicza Av. 30, 30-059 Krakow, Poland; partyka@agh.edu.pl (J.P.); kozien@agh.edu.pl (D.K.); pantak@agh.edu.pl (P.P.)

* Correspondence: kpasiut@agh.edu.pl

Abstract: The present work describes test results for glass crystal materials based on the $\text{SiO}_2\text{-Al}_2\text{O}_3\text{-MgO-K}_2\text{O}$ system after 5, 10, 15, and 20 wt.% zinc oxide was added. The glazing analysis involved determining the effect of the additive on the characteristic temperatures and properties of the surface obtained, such as color, gloss, and roughness, as expressed by a Ra parameter. The obtained glazes were also analyzed for changes in phase composition (quantitative and qualitative XRD tests), changes in microstructure (based on images obtained with a scanning electron microscope), and structure (based on analyses and decomposition of spectra obtained using mid-infrared spectroscopy). As a result, the maximum addition of zinc oxide provided the best results.

Keywords: glazes; structure; willemite; forsterite



Citation: Pasiut, K.; Partyka, J.; Kozień, D.; Pańtak, P. Impact of Zinc Oxide on the Structure and Surface Properties of Magnesium–Potassium Glass–Crystalline Glazes. *Crystals* **2024**, *14*, 456. <https://doi.org/10.3390/cryst14050456>

Academic Editor: Yang Bai

Received: 31 March 2024

Revised: 3 May 2024

Accepted: 8 May 2024

Published: 11 May 2024



Copyright: © 2024 by the authors. Licensee MDPI, Basel, Switzerland. This article is an open access article distributed under the terms and conditions of the Creative Commons Attribution (CC BY) license (<https://creativecommons.org/licenses/by/4.0/>).

1. Introduction

Glazes are materials used to protect the body from external factors. Their presence affects the product's properties, which are important for its functionality. Depending on their use, these parameters can vary; different requirements are placed on glazes for floor tiles than on sanitary ware or tableware ceramics due to their use for a specific purpose [1–6].

Ceramic glazes currently used in products are classified as composite materials because they consist of an amorphous phase and (one or several) crystalline phases (glass–crystalline materials). The presence of crystals in the structure of the material is advantageous because they meet the new requirements placed on glazes by improving their properties and parameters, similar to those of other composite materials [1,5,6].

Obtaining a glass–crystalline material requires a large number of ingredients that contribute to the production of glazes with a lower firing temperature (compared to glasses). A large number of components results in greater system complexity, making it difficult to design new glazes that meet the requirements. Furthermore, the crystallization processes that occur in the glazes, often in several stages, make it almost impossible to accurately predict the properties of the glazes obtained. For this reason, empirical research is necessary based on existing knowledge about specific groups of glazes [1,4,6–8].

Obtaining the desired crystalline phases in a multi-component oxide system, despite the presence of the required components, may not be easy. The presence of some oxides hinders crystal formation by changing the viscosity and reducing the ions' speed of movement in the system. A factor that significantly influences crystallization is the presence of alkali oxides, which act as fluxes in glazes. This interaction involves the creation of systems with other glaze components, characterized by a significant reduction in temperature at which the first portions of the liquid phase appear [1,3,4,7,9].

One of the oxides added to glazes is zinc oxide, which has a fluxing effect above 1000 °C. When added in smaller amounts, it increases the gloss of the surface, but its presence in larger amounts may cause surface crystallization and a dull surface. An

interesting aspect of adding zinc oxide to glazes is the possibility of obtaining a silicate known as willemite. This is a crystalline phase that, if occurring in the form of large crystals, provides the product with decorative value. Obtaining large willemite crystals is quite difficult and requires a firing curve with several cooling and heating phases for optimal crystallite growth. Research on zinc glazes is still ongoing due to the relatively wide use of this oxide in industry and ceramic factories. It also reduces surface properties, such as chemical resistance and mechanical strength. The addition of zinc oxide to glazes affects the color of the glaze when pigments are used, and the final color of underglaze paints [9–25].

The presented work analyzes the impact of adding zinc oxide to a simple tetraoxide glazing system, $\text{SiO}_2\text{-Al}_2\text{O}_3\text{-MgO-K}_2\text{O}$, to which zinc oxide was added in four different amounts: 5, 10, 15, and 20 wt.%. Such a simple oxide system allowed us to determine the changes occurring in enamel, in which magnesium oxide (MgO) and potassium oxide (K_2O) play the main roles. Four zinc oxide concentrations were added to the analyzed system to systematically track changes in parameters and material properties. This work aimed to determine whether willemite crystallization is possible in glazes with high magnesium and potassium content and how the addition of zinc oxide affects the structure, microstructure, and surface properties of the glazes. The results obtained will allow us to understand the processes that occur in this type of system, making it easier to design and modify glazes with similar characteristics.

2. Materials and Methods

The compositions of the glazes were designed based on the Seger composition of glazes from a fine ceramic plant. Four amounts of zinc oxide were added to these glazes: 5, 10, 15, and 20 wt.%. Glazes without the addition of zinc oxide were also prepared as base glazes.

Glazes were prepared by weighing natural raw materials: quartz flour MK-40 (Strzeblowskie Kopalnie Surowcy Mineralnych, Sobótka, Poland), KOC kaolin (Surmin Kaolin, Nowogrodziec, Poland), Quantum potassium feldspar DS (Sibelco, India), talc (Luzenac, Austria), and zinc oxide (Huta Oława, Oława, Poland) according to working recipes calculated based on the above assumptions. The selection of raw materials was determined based on their use in the ceramics industry in Poland.

The raw materials were wet-milled on a Gabriella planetary grinder for 30 min. Each glaze was weighed at 400 g, to which grinding medium and water were added to the raw materials: grinding medium:water = 1:1:0.8. After grinding, the glaze suspension was sprayed onto previously prepared bisque pellets with a diameter of 5 cm. Approximately 5 g of glaze was applied to each lozenge and the remaining part was dried. The samples were also prepared from dry raw glaze by filling bisque containers with approximately 50 g of glaze.

The prepared glaze samples (glazed pellets and containers with raw glaze) were fired in a laboratory chamber furnace. The firing time was 14 h, with the glaze held for 30 min at a maximum temperature of 1240 °C.

The raw glaze was used to mark characteristic temperatures using hot-stage microscopy. Each glaze sample was pressed into a pellet on a hand press and then placed onto an HSM Misura 3 high-temperature microscope on an alundum stand. The sample was heated to a temperature 10 degrees higher than the glaze flow temperature, at a heating rate of 10 deg/min. Characteristic temperatures were determined based on the recorded geometric dimensions of the samples. Based on the height measurements of the samples (measurements beginning at $h = 100\%$), data showing the shrinkage of the samples during the sintering process were obtained.

The fired glazes in the containers were cut into smaller pieces. Some were crushed to powder with a grade of less than 63 μm . The glazes were ground in an agate mortar and sifted through a 63 μm sieve. This powder was used to determine its chemical and phase composition and for structural studies in the mid-infrared range.

Chemical analysis of the fired glazes was performed using wavelength-dispersive X-ray fluorescence spectroscopy. The test was carried out using a WDXRF Axios mAX spectrometer equipped with a 4kW Rh tube from PANalytical.

The phase composition (qualitative and quantitative) of the tested glazes was determined by XRD. The test was performed using a Philips X-Pert Pro X-ray diffractometer. The device is equipped with a ceramic X-ray tube with a copper anode, which emits X-ray radiation with a wavelength of $\lambda = 1.540 \text{ \AA}$, and a proportional detector (PW3011/20) with an angular range of 2θ from 5° to 80° . Quantitative analysis was performed using the internal standard method, selected empirically. As an internal standard for quantitative analysis, 3% aluminum oxide ($\alpha\text{-Al}_2\text{O}_3$) Martoxid MDS-6 was introduced into the samples. The analysis of the diffractograms (quantitative and qualitative) was performed using the HighScore Plus program. The quantitative contribution of the crystalline phases was performed using the Rietveld method.

Research was carried out in the mid-infrared range with the KBr pellet melting technique. Measurements were carried out using a Vertex 70v Fourier spectrometer from Bruker Optics (Billerica, MA, USA) ranging from 1600 cm^{-1} to 400 cm^{-1} with a resolving power of 4 cm^{-1} and 128 scans. The obtained spectra were decomposed using the Bruker Opus 7.2 program. Optics Poland provided component bands.

Using fired and cut pieces of the glazes, polished samples were prepared. Each of them was etched with a 40% hydrofluoric acid solution to remove the amorphous phase. The digestion time for each sample was 30 s, after which they were rinsed with distilled water. The samples were subjected to microstructure observations using a ThermoFisher Scientific Apero 2 scanning electron microscope (ThermoFisher Scientific, Waltham, MA, USA). Phase identification was performed using the EDAX adapter and Apex software.

Glaze surface parameters were determined based on the glazed and fired pellets. The color was determined using a 3Color colorimeter; the data obtained were presented in the CIE $L^*a^*b^*$ system. Gloss was determined using an Elcometer 406L gloss meter at an incidence angle of 60° . Surface roughness was measured using an Olympus LEXT OLS4000 confocal laser microscope.

3. Results and Discussion

3.1. Chemical Analysis (XRF)

The results of the chemical analysis using X-ray fluorescence spectroscopy are presented in Table 1. The percentages obtained for each oxide (except zinc oxide) were averaged and converted into a number of moles for each oxide. Then, they were grouped according to the role they play in the enamel (Segger formula). The values obtained were presented as the ratio of the mole fractions of $\text{SiO}_2/\text{Al}_2\text{O}_3$ (oxides composing the aluminosilicate oxide skeleton of the amorphous phase), the number of moles for flux oxides (MgO and K_2O), and the percentage of added zinc oxide. According to these results, glazes with compositions consistent with those designed were produced.

Table 1. Chemical composition results of the fired samples ($\text{SiO}_2/\text{Al}_2\text{O}_3$ molar ratio, MgO , K_2O molar, and ZnO wt.%).

Sample	Segger Formula			Amount of ZnO [wt.%]
	$\text{SiO}_2/\text{Al}_2\text{O}_3$	MgO	K_2O	
Zn0				0
Zn5				4.9 ± 0.1
Zn10	6.98 ± 0.03	0.65 ± 0.01	0.37 ± 0.03	10.6 ± 0.2
Zn15				15.1 ± 0.4
Zn20				20.4 ± 0.3

3.2. Characteristic Temperatures (HSM)

Based on the measurements, movies were created showing changes in the samples, from which characteristic temperatures could be determined (Figure 1). The marking error is one degree. The height values were also obtained from measurements during sample heating. These data indicate how quickly changes occur in the samples, which is directly related to the liquid phase amounts in the samples (Figure 2).

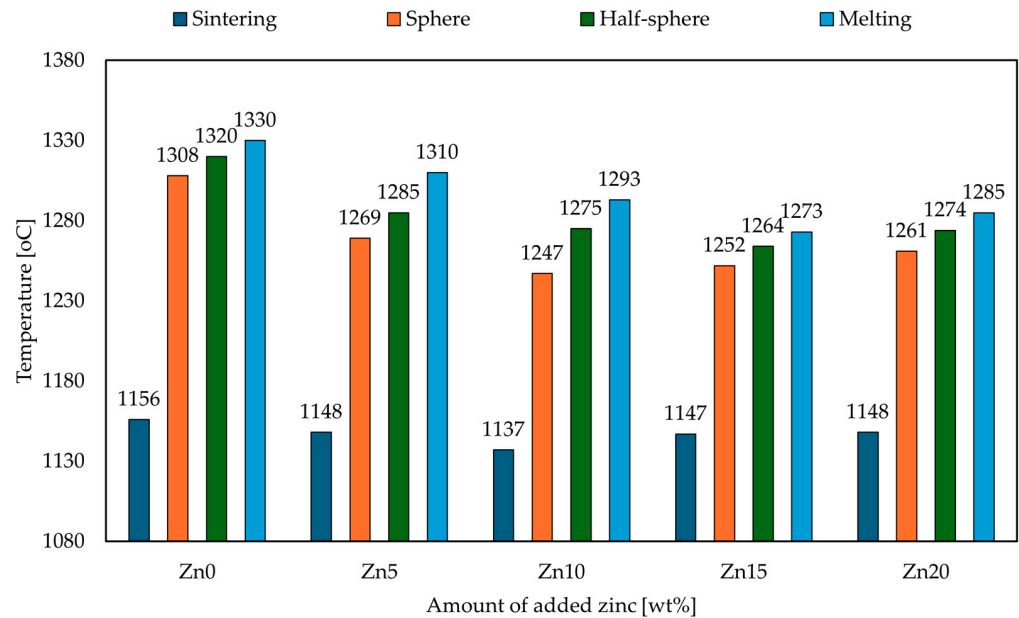


Figure 1. Characteristic temperatures of the glazes analyzed.

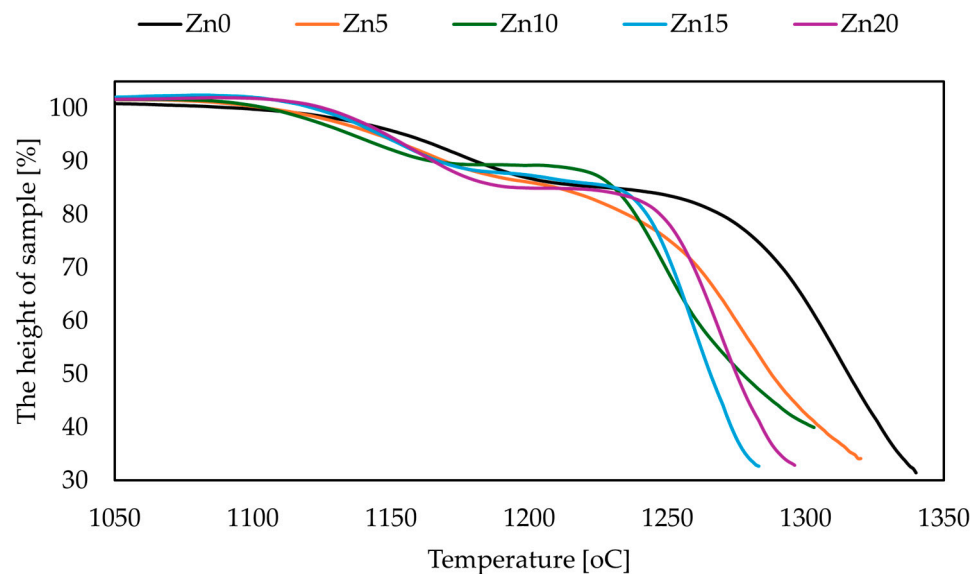


Figure 2. The height of a sample as a function of temperature.

The characteristic temperature results showed that zinc oxide addition did not significantly affect sintering temperatures. A slight reduction was observed, with no proportional relationship. The lowest sintering temperature was obtained for glazes with 10 wt.% (Zn10) of added zinc oxide. In the case of other characteristic temperatures, the addition of zinc oxide demonstrated similar effects. The decrease caused by zinc oxide addition was not proportional to the amount of zinc oxide added. The lowest characteristic temperatures

were obtained for sphere temperature, hemisphere temperature, and reflow temperature for the Zn10, Zn15, and Zn15 glazes, respectively.

Such values indicate that zinc oxide flux reduces characteristic temperatures to some extent. Added high amounts of zinc oxide do not provide any benefits in terms of lowering characteristic temperatures; therefore, it is economically unprofitable. The most optimal additive for reducing characteristic temperatures appears to be between 10 and 15 wt.% zinc oxide. The addition of such an amount allows zinc oxide to perform as an optimal flux. Furthermore, the addition of higher amounts does not affect the fluxing effect, but may already have a glass-forming effect, which has been confirmed in some studies [11–16].

Sample height changes for the glazes analyzed were similar, but their rates differed, especially above 1200 °C. The slowest height drop was visible for glazes without the addition of zinc oxide, whereas the fastest was visible for the Zn15 glaze. These results indicated that the effect of zinc oxide as a flux intensifies above this temperature compared to zinc oxide addition at 15 wt.%, which increases sintering process speed.

3.3. Phase Composition (XRD)

The phase composition of the glazes analyzed is presented in Table 2 and Figure 3. Three different crystalline phases were observed in the glazes. The first was forsterite (ICSD 98-000-9685) [26], which is a magnesium silicate that only appears as a crystalline phase in glazes with no or low calcium oxide content. In the group of glazes, a decrease in forsterite was observed when increasing amounts of zinc oxide were added. For the Zn15 and Zn20 glazes, the presence of this crystalline phase was not found. The second crystalline phase that appeared in the glazes was the α -quartz phase (ICSD 98-001-6331) [27], which probably comprises the so-called residual quartz that did not dissolve during the firing process. As in the case of forsterite, the amount of quartz decreases with increased amounts of zinc oxide in the glaze, particularly in 15 and 20 wt.% additions. Its presence was not detected in these glaze samples. The third crystalline phase that appeared in glazes was willemite (ICSD 98-000-2425) [28], which is a zinc silicate that appears as a crystalline phase in glazes where zinc is present. However, the presence of the necessary ingredients for crystallization does not determine the certainty of this crystalline phase's appearance. Willemite was found in the glaze even with the lowest amount of zinc oxide, and as the amount of this oxide in the glaze increased, a proportional increase in zinc silicate content was found during the crystalline phase.

Table 2. Phase composition of the analyzed glazes.

Glaze	Forsterite [vol.%]	Quartz [vol.%]	Willemite [vol.%]	Amorphous Phase [vol.%]
Zn0	21.9	18.0	-	60.1
Zn5	13.9	12.5	2.4	71.2
Zn10	10.0	6.2	5.5	78.3
Zn15	-	trace	7.8	92.2
Zn20	-	trace	11.8	88.2

The amount of crystalline phase increased with an increased amount of added zinc oxide, except for the Zn20 glaze, where the amount of the amorphous phase was slightly lower than in the Zn15 glaze at 88.2 and 92.2 vol.%, respectively. These findings indicated that despite the appearance of a new crystalline phase, willemite, and the disappearance of forsterite and quartz, zinc oxide causes the formation of a more reactive liquid phase, which dissolves residual quartz and stops the crystallization processes of other crystalline phases, including forsterite.

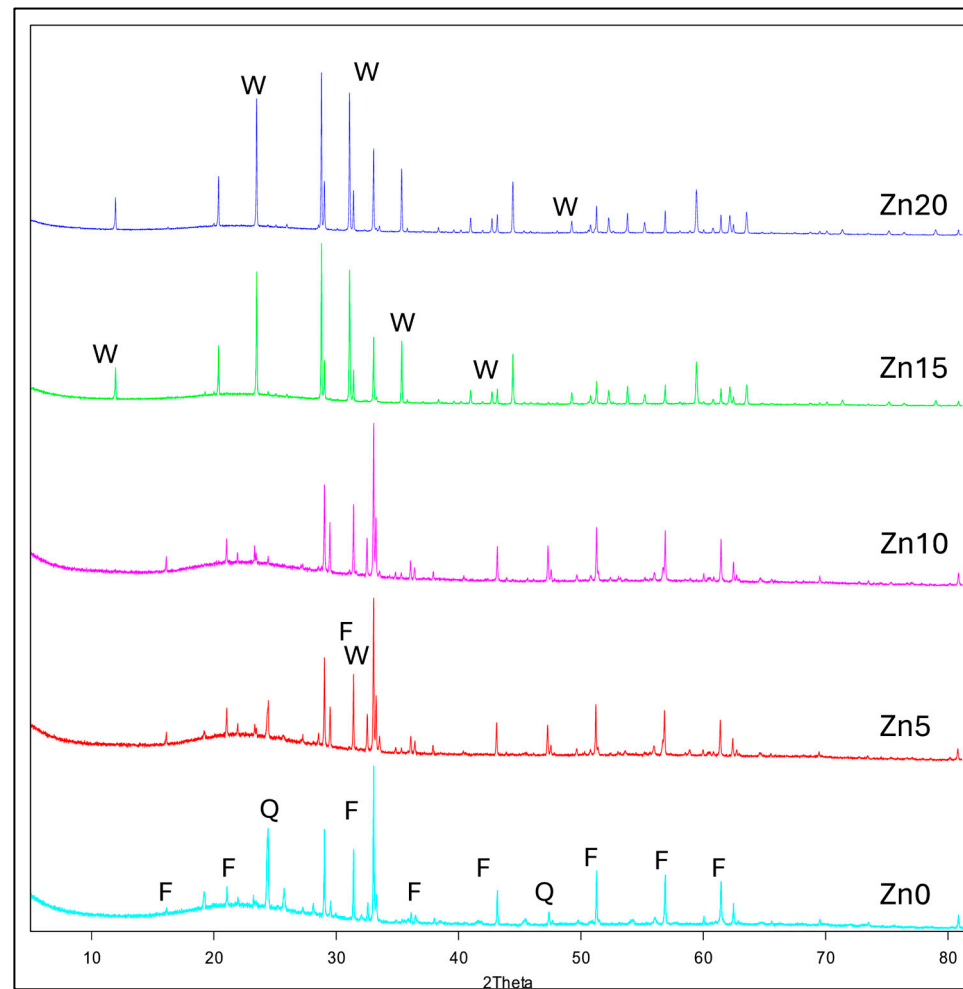


Figure 3. XRD pattern of the glazes analyzed (W = willemite, Q = quartz, F = forsterite).

3.4. Microstructure (SEM)

The microstructures of the obtained glazes were observed on previously etched samples. The shape of the obtained crystals can be seen by removing the amorphous phase. Observations were made at various magnifications, but due to the size of the obtained crystals, analysis was only possible at 3000 times magnification. Figures 4–8 show micrographs obtained during analysis.

For the Zn0 glaze (Figure 4), the presence of cuboid-shaped forsterite crystals with well-developed walls was observed. The crystal sizes obtained were in the range of several micrometers. The forsterite crystals were not evenly distributed across the entire surface but grouped into clusters. Residual quartz crystals were also observed in sizes between 10 and 30 μm .

The microstructure of the Zn5 glaze showed similarity in terms of forsterite crystal clustering and size. Glazes with a zinc oxide addition of 5 wt.% showed much smaller forsterite crystals, whose shape was slightly different from that observed in Zn0 glazes. In this case, the edges of the crystallites were not as sharp and distinct, indicating that they may not have been as well-developed as in the previous glaze. Residual quartz crystals were also observed in this glaze. However, no willemite crystals were observed according to phase composition analysis (Table 2). This finding may be due to fewer amounts in the sample or their small size.



Figure 4. Microstructure of Zn0 glazes at 5000× magnification with EDS analysis.

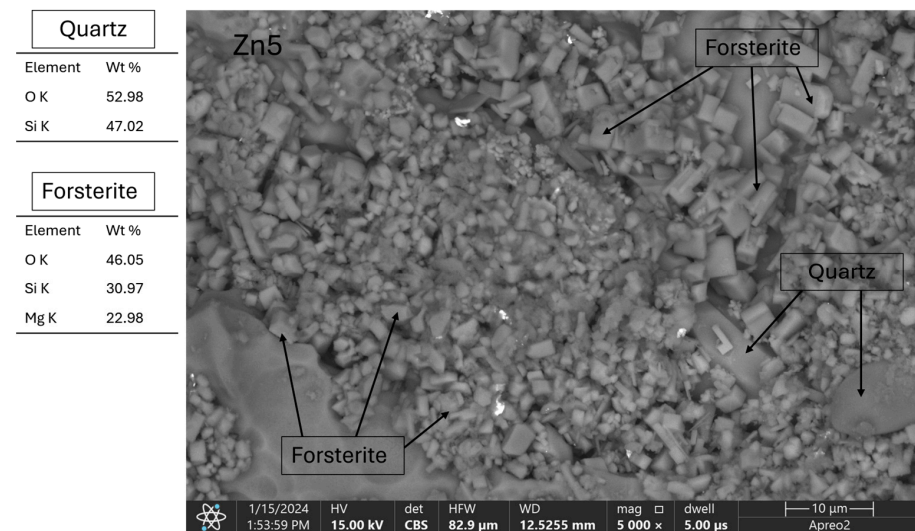


Figure 5. Microstructure of Zn5 glazes at 5000× magnification with EDS analysis.

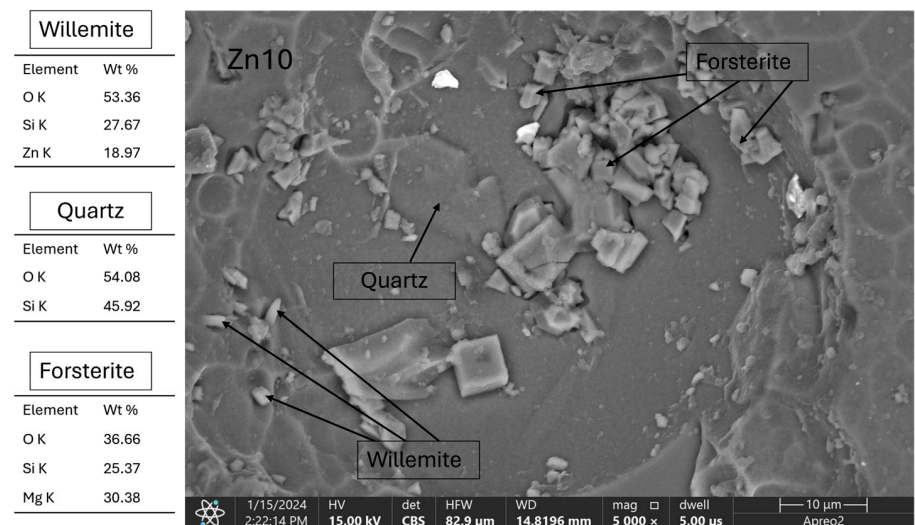


Figure 6. Microstructure of Zn10 glazes at 5000× magnification with EDS analysis.

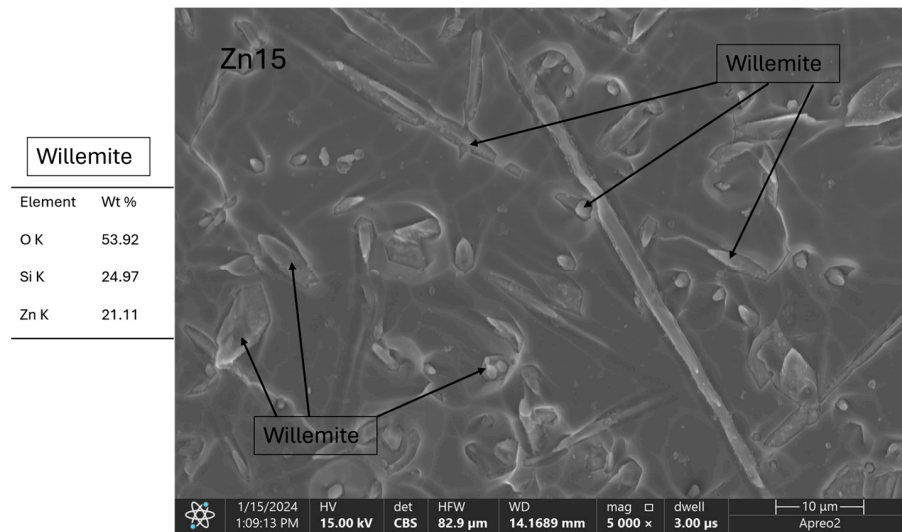


Figure 7. Microstructure of Zn15 glazes at 5000× magnification with EDS analysis.

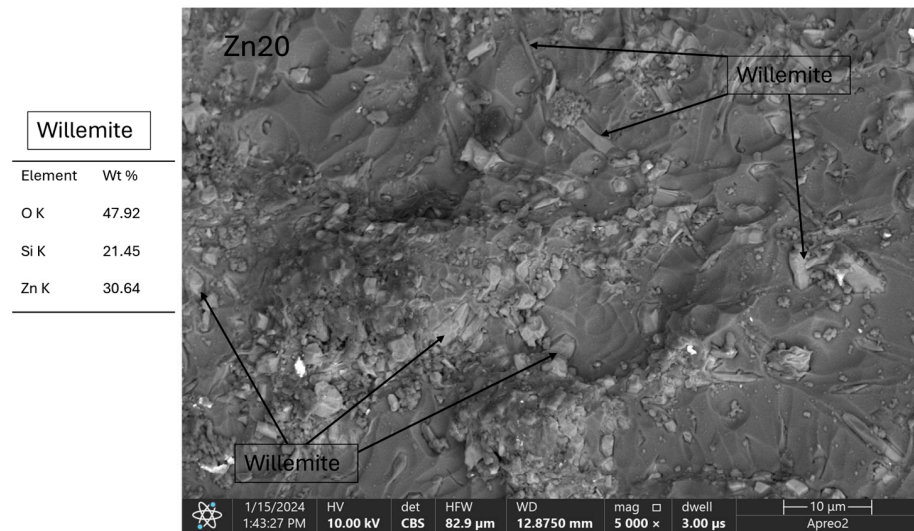


Figure 8. Microstructure of Zn20 glazes at 5000× magnification with EDS analysis.

In the Zn10 glaze, forsterite crystals were observed in much smaller amounts than in the previous glazes, as confirmed by phase composition analysis (Table 2). These crystals had various sizes, some slightly larger than 10 μm. As in the Zn5 glaze, the crystal edges were not clear and sharp, which may be because the crystal phase of forsterite is defective, making it less resistant to concentrated hydrofluoric acid. The second crystalline phase had willemite crystals, whose shape, characteristic of this crystalline phase, crystallized in the form of needles. As a result of the digestion of the sample, fragments of long crystals can be observed. Forsterite and willemite crystal phases occurred next to each other in clusters.

In the Zn15 glaze, only willemite crystals with characteristic needle shapes were observed. They had different lengths and non-uniform orientations, with willemite crystals oriented in different directions. In addition to willemite needles, willemite crystals with a slightly different shape, i.e., polyhedra, were also observed.

Both types of willemite were more visible in glazes with the addition of 20 wt.% ZnO. In addition to needles, crystals in the form of well-developed polyhedra were also observed. Unlike the other samples, the distribution of willemite crystals is relatively uniform in all of the analyzed samples.

3.5. Structure Analysis (MIR)

To analyze changes in structure based on spectra obtained in the mid-IR, decomposition is required. The decomposition of the obtained spectra into component bands helps assign individual component bands to vibrations occurring in the structure. It also tracks changes in their position as a function of compositional changes. In the case of materials containing both amorphous and crystalline phases, analyzing changes in structure is difficult because of bond vibrations in crystalline phases. Therefore, comparing the obtained component bands to those present in pure crystalline phases is useful. However, bands originating from bond vibrations in crystalline phases can and often overlap with those originating from bonds in the amorphous phase.

Analysis of the phase composition showed three crystalline phases in the tested glazes: forsterite, willemite, and quartz. Figure 9 shows the spectra of pure crystalline phases [29–31], while Figure 10 shows the glazes' spectra using measurements in the mid-infrared range.

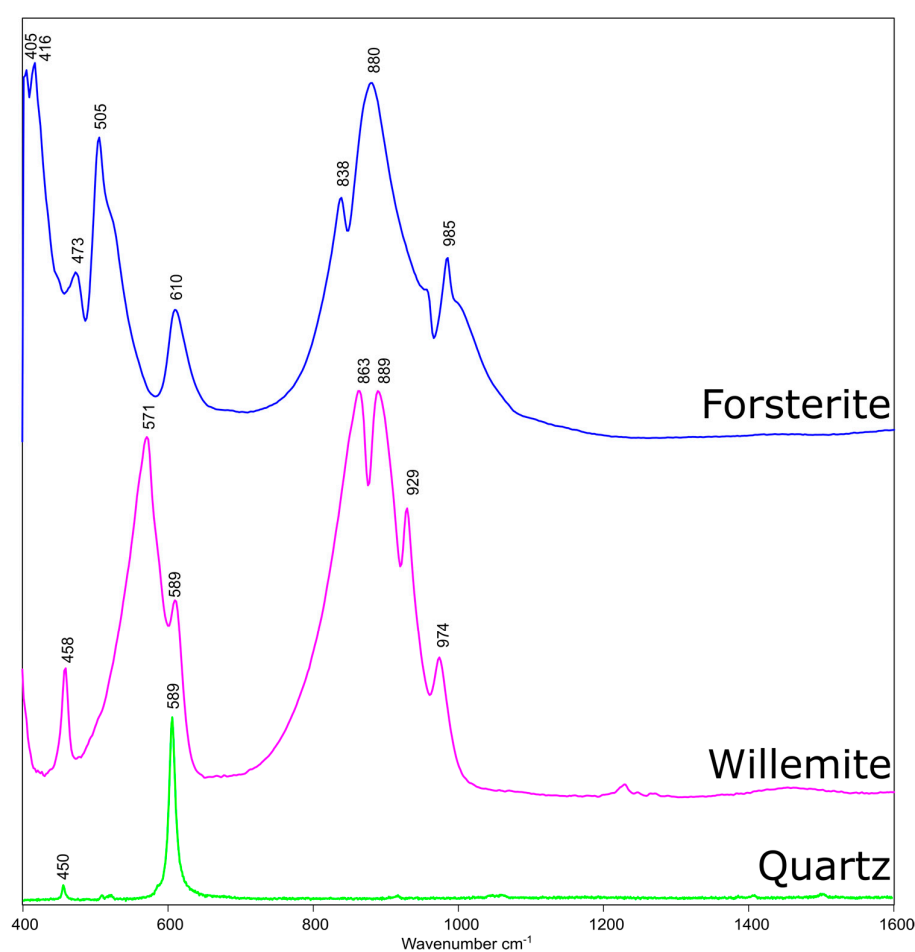


Figure 9. MIR spectra of forsterite, willemite, and quartz [29–31].

Table 3 presents the results of spectra decomposition, including component bands and their descriptions. Bands recorded for the Zn0 glaze at wavenumbers of 466 and 512 cm^{-1} corresponded to a range of bending vibrations for aluminum and silicon–oxygen bridges, respectively. When the position of this group of bands was analyzed after the addition of zinc oxide, a slight change in the position of bands corresponding to the bending vibrations of aluminum oxide bridges was observed. However, in the case of bands corresponding to the bending vibrations of silica bridges, a change in position toward lower wavenumbers was observed, indicating an increase in structural disorder. In the case of Zn0 and Zn5 glazes, both bands may partially originate from vibrations in the forsterite structure [32–35].

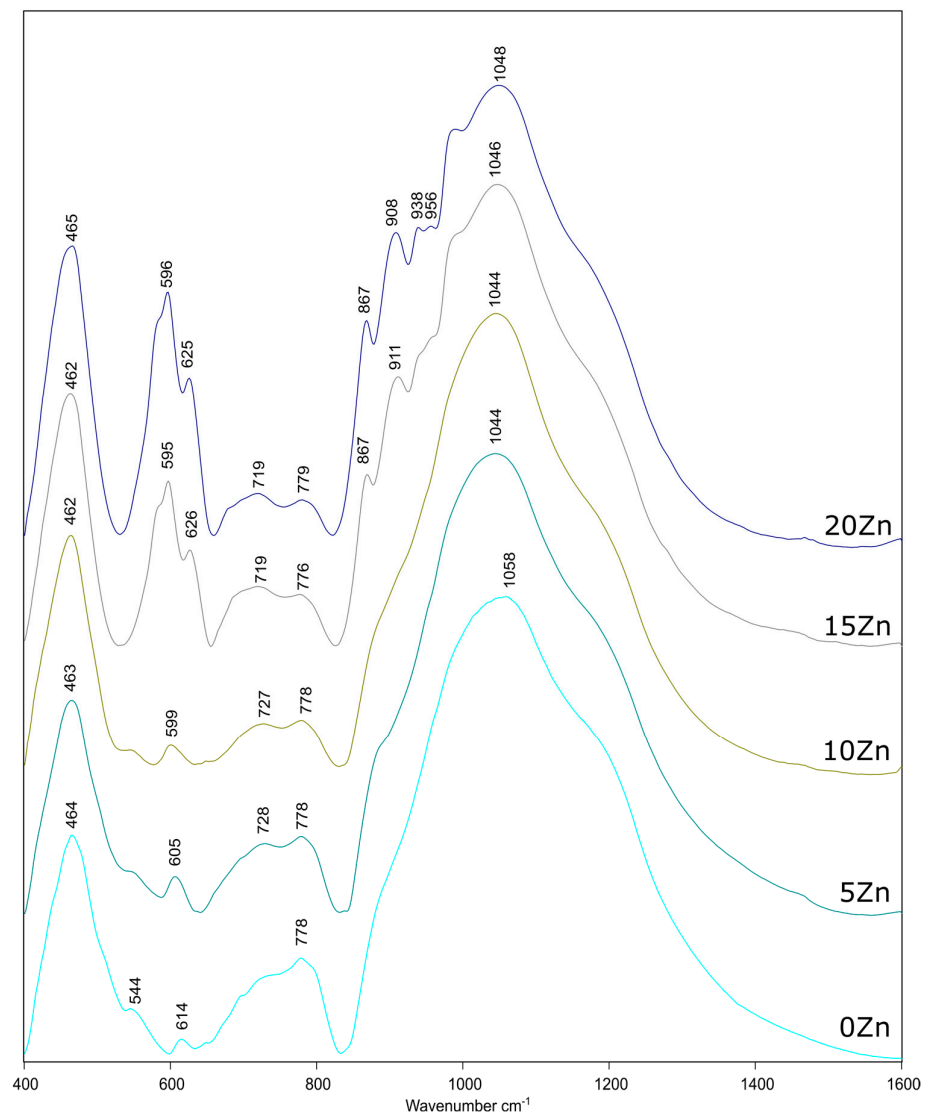


Figure 10. MIR spectra of the glazes analyzed.

Table 3. List of component bands after the decomposition process of the analyzed glazes.

Zn0	Zn5	Zn10	Zn15	Zn20	Band Ascription	Source
466	461	460	460	463	δ (O-Al-O)	[32–35]
512	498	497	487	495	δ (O-Si-O)	[32–35]
549	545	544	590	589	Ring structure	[36,37]
615	608	602	598	598		
			630	629		
709	689	708	684	681	ν (Si-O-Al)	[32–35]
752	739	733	722	718	ν (Si-O-Si)	
782	781	780	773	774		
804	803	803	796	795		
887	883	871	863	863	ν Al-O-[NB]	[32–34]
		902	907	906	willemite	[30]
			940	940	willemite	[30]
949	947	957	955	956	ν Si-O-[NB]	[32–34]
			978	978	willemite	[30]
1015	1022	1013	1022	1014	ν Si-O-Al	[32–34]
1082	1088	1073	1067	1062	ν Si-O-Si	
1190	1183	1166	1170	1169	ν Si=O	

The next group of bands corresponded to vibrations of multi-membered aluminum and silicoid rings. In this group, slight changes in the band positions were observed, both toward higher and lower wave numbers, indicating depolymerization of the structure and polymerization. In this group, new bands related to the presence of the willemite crystalline phase were also observed for Zn15 and Zn20 glazes (Figure 9). The presence of new bands indicates that the structure has formed more bonds and is, therefore, more ordered [34,36,37].

The next group of bands are bands of symmetric stretching vibrations for Si-O-Si and Si-O-Al bridges. In the case of bands corresponding to symmetric stretching vibrations of Si-O-Al bridges, a shift in this band toward lower wave numbers from 752 to 718 cm^{-1} was observed for Zn0 and Zn20 glazes, respectively. Such a shift indicates an increase in structure disorder. In the case of symmetric stretching vibrations for Si-O-Si bridges, a shift in these bands toward lower wave numbers was also observed, but it was not substantial [32–34].

The group of bands from 870 to 1200 cm^{-1} corresponds to a range of asymmetric stretching vibrations for Al-O and Si-O bonds in aluminum and silica tetrahedra. In this group, the range of asymmetric vibrations and stretching vibrations associated with broken aluminum and silica concrete bridges was determined. In the case of bands corresponding to broken aluminum oxide bridges, a shift toward lower wave numbers was observed from 887 to 863 cm^{-1} for Zn0 and Zn20, respectively. In the case of bands corresponding to a range of asymmetric stretching vibrations for broken silicoid bridges, a slight shift toward higher wave numbers was observed, suggesting a process to organize the structure. However, within this group of bands, three additional bands related to the presence of willemite appeared (Figure 9). The wave number range of 1090–1000 cm^{-1} corresponded to the asymmetric stretching vibrations of Si-O(Si) and Si-O(Al). Only in the case of bands corresponding to silica bridges containing bridge bonds was there a significant change in the position of bands toward lower wave numbers. Such a change in position indicates an increase in structural disorder. Note that the location of this band came only from the amorphous phase because no other bands originated from the crystalline phases present in this range [13,15,32–34].

The last group of bands in the analyzed spectra corresponded to Si=O stretching vibrations, indicating defects in the structure, such as silica tetrahedra connected by edges. In the case of this group of bands, the addition of zinc oxide caused this band to shift toward lower wave numbers, indicating an increase in glaze structure disorder.

The described changes in the structure observed during the analysis of the bands after decomposition indicated decomposition and an increase in the structural disorder of the glaze with the addition of zinc oxide. Changes in the positions of the component bands were toward lower wave numbers, indicating an increase in structural disorder. This finding was expected due to the total increase in the amorphous phase in the glazes (Table 2). The amorphous (glassy) phase showed much less order than the crystalline phases, so the total increase in the amount of the amorphous phase should increase the disorder of the entire sample [15,16,33,38].

3.6. Surface Parameters

The surface parameters of the glazes are important from a technological and application point of view. They are important elements for the user, and the obtained surface quality indicates whether the glaze will fulfill its protective role. The most frequently tested surface parameters include color, gloss, and roughness.

The surfaces obtained from the glazes on the fired pellets were characterized by a light shade and could be described as cloudy glazes because they completely covered the ceramic body. No crystalline phases were visible to the naked eye. The surfaces of the glazes differed not only in color but also in gloss.

Surface color tests were performed for each glaze by measuring the color parameters ten times for each sample. The results are presented in Figure 11. Based on the data

obtained, a change in the value of the L^* parameter (brightness) was observed after adding zinc oxide to the glaze. A 5 wt.% addition of ZnO caused the value of this parameter to increase from 79.26 to 88.79, which was the highest value for this parameter out of all glazes tested. For ZnO additions in the amounts of 10 and 15 wt.%, an increase in the brightness value of the glaze color was also observed. The highest addition resulted in the value of the L^* parameter being at the level of the base glaze.

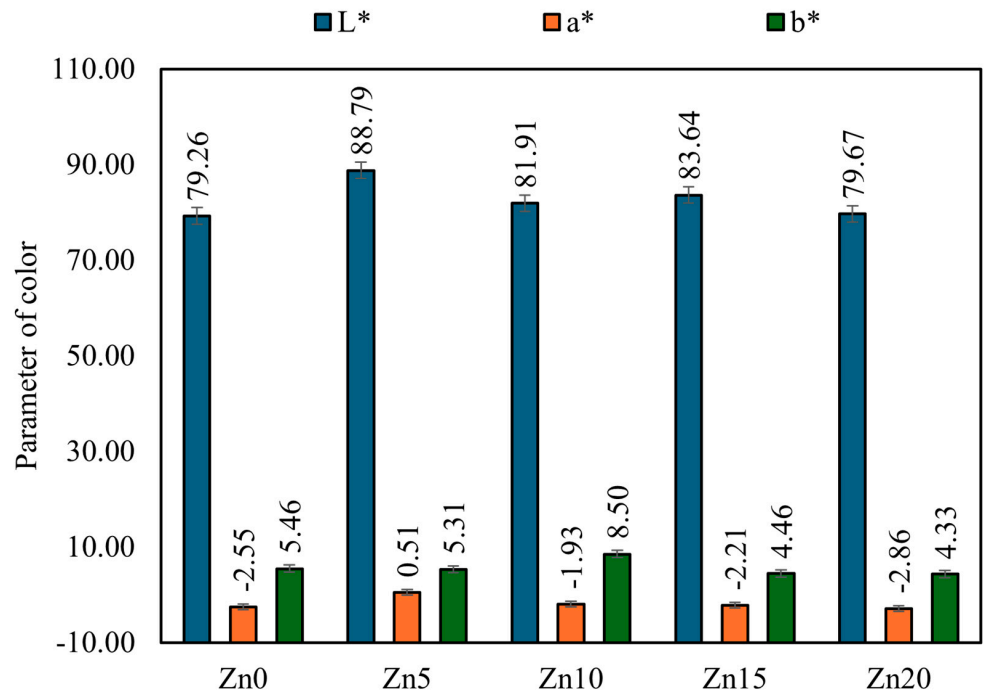


Figure 11. Color of the glazes analyzed.

The addition of zinc oxide also caused changes in the values of parameters a^* and b^* , which are color components. In the case of the a^* parameter, a change toward achromatic color (approaching zero) was observed and was most noticeable after the addition of 5 and 10 wt.% zinc oxide. These changes were minor in the case of Zn15 and Zn20 glazes; and, they were within the measurement error limit. All the values obtained for parameter a^* , except for glaze Zn5, had negative values, and indicate the green color component. Red color components in the glaze indicates positive values. The b^* parameter showed greater variability in the chemical composition of the glaze. The addition of zinc oxide in the amount of 5 wt.% did not cause a significant change in the value of this parameter, whereas another sample with 10 wt.% ZnO increased the value of this parameter by three units and the amount of the yellow color component in this glaze. Further additions, namely 15 and 20 wt.% ZnO, caused a slight reduction in the value of parameter b^* from 4.46 to 4.33 for the Zn15 and Zn20 glazes, respectively. Moreover, the yellow color component in these glazes was reduced.

Upon analyzing the results, it can be concluded that the presence of the crystalline willemite phase in the Zn15 and Zn20 glazes, combined with a significant share of the amorphous phase, minimizes the brightness value of the glaze. From a technological and application point of view, zinc glazes with high zinc oxide content do not result in a light-colored surface.

Roughness and gloss are parameters that characterize surface quality, with each parameter describing the quality of the obtained surface in different ways. Gloss measurements were performed for each glaze by measuring the surface gloss ten times. Surface roughness measurement was determined by linear measurement of the R_a parameter. Twelve such

measurements were obtained for each glaze. The gloss and roughness results are shown in Figure 12.

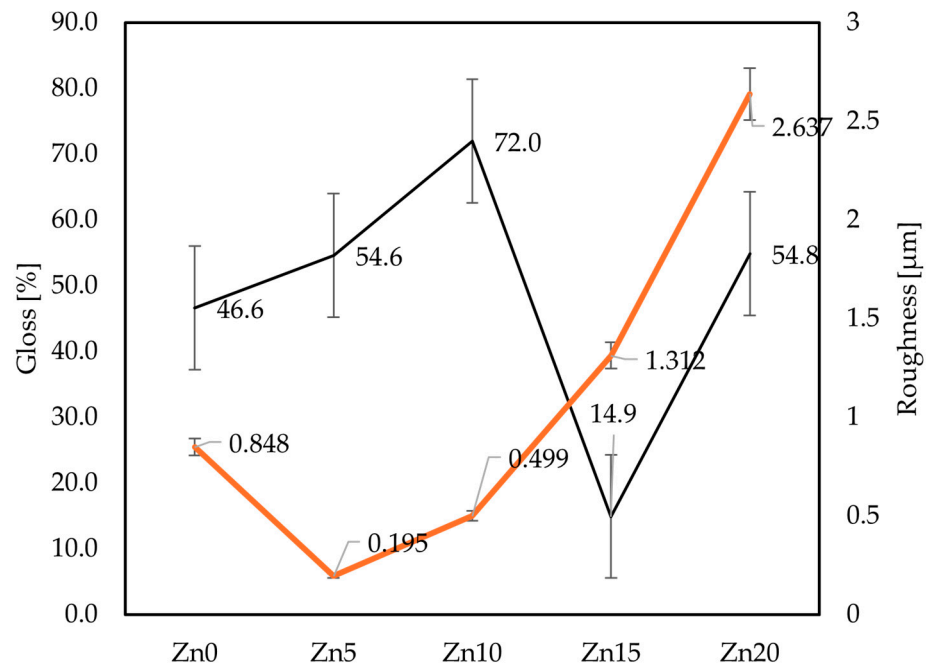


Figure 12. Gloss and roughness of the glazes analyzed (gloss).

The gloss measurements confirmed macroscopic observations of the glaze surfaces. The surfaces obtained differed in gloss. The shiniest surface was obtained from the Zn10 glaze (25.4% increase over the Zn0 glaze). In general, zinc oxide addition affected glaze gloss, but this change was not linear. The gloss change for the Zn5 and Zn20 glazes is insignificant compared to the base glaze, while the addition of 15 wt.% zinc oxide caused a significant decrease in gloss value, producing a glaze with a matte surface and 14.9% gloss component.

Surface roughness measurements showed that zinc oxide additions of 5 and 10 wt.% caused a decrease in this parameter, i.e., fewer surface profile deviations from the average. However, higher amounts of zinc oxide increased the Ra parameter by 0.464 and 1.789 for Zn15 and Zn20 glazes, respectively. In the case of the last glaze, this increase was very significant.

The results obtained from the surfaces' characteristic parameters indicate that the optimal addition of zinc oxide, which improves the quality of the obtained surface, is 10 wt.% ZnO. Changes in surface gloss may be caused by a change in the number of crystalline phases and an increase in amorphous phases, the larger amount of which produces better light reflections on the surface, i.e., better gloss. However, a decrease in gloss value with a simultaneous increase in amorphous phases may be associated with the crystal arrangement, whose location near the glaze surface affects this parameter's value.

The measured surface roughness indicates that the surface quality deteriorates due to the increasing deviation of the profile from the average. The Ra parameter provides information on how uneven the surface is, that is, whether the glaze is more or less smooth. This parameter is important in the context of glaze usage; the lower the value of the Ra parameter, the more uniform the glaze surface (fewer deviations from the average). Not only is it easier to maintain and clean, but its mechanical strength and corrosion resistance are greater.

4. Conclusions

This work examined the effects of zinc oxide addition on glazes using the $\text{SiO}_2\text{-Al}_2\text{O}_3\text{-MgO-K}_2\text{O}$ system. Zinc oxide was added at 5, 10, 15, and 20 wt.%. Parameters such as characteristic temperature, chemical composition, and phase composition were measured. Changes in microstructure and surface parameters, such as color, gloss, and roughness, were also determined. Based on these tests and analyses, the Zn10 glaze had the greatest application potential due to its optimized parameters.

The fluxing effect of zinc oxide was also confirmed but was not directly proportional to the zinc oxide amount added. The presence of two interesting crystalline phases of forsterite was indicated. During zinc oxide addition, willemite crystals appeared, whose shape was described in the microstructure analysis of the fired glazes. Observed changes in the shape of forsterite crystals may indicate defects in their structure. By contrast, changes in the shape of willemite crystals indicate a more developed microstructure in this crystalline phase with increased zinc oxide in the glaze composition. Our structural analysis confirmed that zinc oxide has a depolymerizing effect and increases the amount of the amorphous phase in the glaze in increased amounts.

Author Contributions: Conceptualization, K.P.; methodology, K.P., J.P., D.K. and P.P.; formal analysis, K.P.; investigation, K.P. writing—original draft preparation, K.P.; writing—review and editing, K.P. All authors have read and agreed to the published version of the manuscript.

Funding: Polish Ministry of Education and Science for the AGH University of Science and Technology in Krakow (Project No. 16.16.160.557).

Data Availability Statement: The raw data supporting the conclusions of this article will be made available by the authors on request.

Acknowledgments: SEM investigations were supported by the program Excellence Initiative—Research University for the AGH University of Krakow, Grant ID 1449 (PI: M. Ziabka).

Conflicts of Interest: The authors declare no conflicts of interest.

References

1. Eppler, R.A.; Eppler, D.R. *Glazes and Glass Coatings*; American Ceramic Society: Westerville, OH, USA, 2000.
2. Shaw, K. *Ceramic Glazes*; Elsevier Publishing Co., Ltd.: Amsterdam, The Netherlands, 1972.
3. Gosh, S.; Pal, K.S.; Dandapat, N.; Ghosh, J.; Datta, S. Glass-ceramic glazes for future generation floor tiles. *J. Eur. Ceram. Soc.* **2013**, *33*, 935–942. [[CrossRef](#)]
4. Holand, W.; Beall, G.H. *Glass-Ceramic Technology*; Wiley: Hoboken, NJ, USA, 2012.
5. Brow, R.K. *Glasses and Glass-Ceramics*; Butterworth-Heinemann: Oxford, UK, 1993.
6. Taylor, J.R.; Bull, A.C. *Ceramics Glaze Technology*; Pergamon Press: Oxford, UK, 1986.
7. Manfredini, T. Ceramic tile glazes: Design, trends and applications. In Proceedings of the Euro Ceramics VII: 7th Conference Exhibition of the European Ceramic Society, Brugge, Belgium, 9–13 September 2001.
8. Manfredini, T.; Pellacani, G.C.; Rincon, M. *Glass-Ceramic Materials Fundamentals and Applications*; Series of Monographs on Materials Science Engineering and Technology; Mucchi Editore: Modena, Italy, 1997.
9. Yaowakulpattana, P.; Wakasugi, T.; Kondo, S.; Kadono, K. Effect of alkaline and alkaline-earth metal oxides addition on the glass formation and crystallization of $\text{ZnO-Al}_2\text{O}_3\text{-SiO}_2$ glasses. *Eng. J.* **2015**, *19*, 21–33. [[CrossRef](#)]
10. Partyka, J.; Pasiut, K.; Jeleń, P.; Lesniak, M.; Sitarz, M. Comparison of the impact of the addition of three alkaline earth metal oxides BaO, SrO and ZnO on sintering of glass-ceramic glazes from the $\text{SiO}_2\text{-Al}_2\text{O}_3\text{-CaO-MgO-Na}_2\text{O-K}_2\text{O}$ system. *J. Therm. Anal. Calorim.* **2019**, *138*, 4341–4347. [[CrossRef](#)]
11. Lesniak, M.; Partyka, J.; Gajek, M.; Sitarz, M. FTIR and MAS NMR study of the zinc aluminosilicate ceramic glazes. *J. Mol. Struct.* **2018**, *1171*, 17–24. [[CrossRef](#)]
12. Gajek, M.; Partyka, J.; Leśniak, M.; Rapacz-Kmita, A.; Wójcik, Ł. Gahanite white colour glazes in $\text{ZnO-R}_2\text{O-RO-Al}_2\text{O}_3\text{-SiO}_2$ system. *Ceram. Int.* **2018**, *44*, 15845–15850. [[CrossRef](#)]
13. Leśniak, M.; Partyka, J.; Sitarz, M. Impact of ZnO on the structure of aluminosilicate glazes. *J. Mol. Struct.* **2016**, *1126*, 251–258. [[CrossRef](#)]
14. Partyka, J.; Leśniak, M. Preparation of glass-ceramic glazes in the $\text{SiO}_2\text{-Al}_2\text{O}_3\text{-CaO-MgO-K}_2\text{O-Na}_2\text{O-ZnO}$ system by variable content of ZnO. *Ceram. Int.* **2016**, *42*, 8513–8524. [[CrossRef](#)]
15. Leśniak, M.; Gajek, M.; Partyka, J.; Sitarz, M. Structure and thermal properties of the fritted glazes in $\text{SiO}_2\text{-Al}_2\text{O}_3\text{-CaO-MgO-Na}_2\text{O-K}_2\text{O-ZnO}$ system. *J. Therm. Anal. Calorim.* **2017**, *130*, 165–176. [[CrossRef](#)]

16. Leśniak, M.; Jastrzębski, W.; Gajek, M.; Partyka, J.; Dorosz, D.; Sitarz, M. The structure of model glasses of the amorphous phase of glass-ceramic glazes from the SiO₂-Al₂O₃-CaO-MgO-Na₂O-K₂O-ZnO system. *J. Non-Cryst. Solids* **2019**, *515*, 125–132. [CrossRef]
17. El-Defrawi, S.A.; Serry, M.A.; El-Fattah, W.I.A.; Weisweiler, W. Microchemistry and microstructure of some opaque glaze/tile interfaces in relation to their physical properties. *Ceram. Int.* **1995**, *21*, 69–75. [CrossRef]
18. Boudeghdegh, K.; Diella, V.; Bernasconi, A.; Roula, A.; Amirouche, Y. Composition effects on the whiteness and physical-mechanical properties of traditional sanitary-ware glaze. *J. Eur. Ceram. Soc.* **2015**, *35*, 3735–3741. [CrossRef]
19. Atkinsin, I.; Anghel, E.M.; Munteanu, C.; Voucescu, M.; Zaharescu, M. ZrO₂ influence on structure and properties of some alkali lime zinc aluminosilicate glass ceramics. *Ceram. Int.* **2014**, *40*, 7337–7344. [CrossRef]
20. Yekta, B.E.; Alizadeh, P.; Rezazadeh, L. Synthesis of glass-ceramic glazes in the ZnO-Al₂O₃-SiO₂-ZrO₂ system. *J. Eur. Ceram. Soc.* **2007**, *27*, 2311–2315. [CrossRef]
21. Bernasconi, A.; Diella, V.; Marinoni, N.; Pavese, A.; Francescon, F. Influence of composition on some industrially relevant properties of traditional sanitary-ware glaze. *Ceram. Int.* **2012**, *38*, 5859–5870. [CrossRef]
22. Cai, J.; Lv, M.; Guan, K.; Sun, Q.; Peng, C.; Wu, J.; Liu, Y. Development of spinel opaque glazes for ceramic tiles. *J. Eur. Ceram. Soc.* **2018**, *38*, 297–302. [CrossRef]
23. Thieme, K.; Thieme, C. Determination of the crystallization mechanism of glasses in the system BaO/SrO/ZnO/SiO₂ with differential scanning calorimetry. *J. Therm. Anal. Calorim.* **2020**, *142*, 1193–1206. [CrossRef]
24. Rudkovskaya, N.V.; Mikhailenko, N.Y. Decorative zinc-containing crystalline glazes for ornamental ceramics (a review). *Glass Ceram.* **2001**, *58*, 387–390. [CrossRef]
25. Smedskjaer, M.M.; Youngman, R.E.; Mauro, J.C. Impact of ZnO on the structure and properties of sodium aluminosilicate glasses: Comparison with alkaline earth oxides. *J. Non-Cryst. Solids* **2013**, *381*, 58. [CrossRef]
26. Smyth, J.R.; Hazen, R.M. The crystal structures of forsterite and hortonolite at several temperatures up to 900 °C. *Am. Mineral.* **1973**, *7–8*, 588–593.
27. D'amour, H.; Denner, W.; Schulz, H. Structure determination of a α -quartz up to 68×10^8 Pa. *Acta Cryst.* **1979**, *B35*, 550–555. [CrossRef]
28. McMuridie, H.F.; Morris, M.C.; Evans, E.H.; Paretzkin, B.; Wong-Ng, W.; Hubbard, C.R. Standard X-Ray diffraction powder patterns from the JCPDS research associateship. *Powder Diffr.* **1986**, *1*, 265–275. [CrossRef]
29. RUFF Spectra. Forsterite R040018. Available online: <https://ruff.info/forsterite/display=default/R040018> (accessed on 20 March 2024).
30. RUFF Spectra. Willemite R050652. Available online: <https://ruff.info/willemite/display=default/R050652> (accessed on 20 March 2024).
31. RUFF Spectra. Quartz R040031. Available online: <https://ruff.info/quartz/display=default/R040031> (accessed on 20 March 2024).
32. Merzbacher, C.I.; mcGrath, K.J.; Higby, P.L. ²⁹Si NMR and infrared reflectance spectroscopy of low-silica calcium aluminosilicate glasses. *J. Non-Cryst. Solids* **1991**, *136*, 249–259. [CrossRef]
33. Furukawa, T.; White, W.B. Vibrational spectra and glass structure. *J. Non-Cryst. Solids* **1980**, *38–39*, 87–92. [CrossRef]
34. Sitarz, M. The structure of simple silicate glasses in the light of Middle Infrared Spectroscopy studies. *J. Non-Cryst. Solids* **2011**, *357*, 1603–1608. [CrossRef]
35. Mozgawa, W.; Sitarz, M.; Rokita, M. Spectroscopic studies of different aluminosilicate structures. *J. Mol. Struct.* **1999**, *511–512*, 251–257. [CrossRef]
36. Sykes, S.; Kubicki, J.D. Four-membered rings in silica and aluminosilicate glasses. *Am. Mineral.* **1996**, *81*, 265–272. [CrossRef]
37. Sitarz, M.; Mozgawa, W.; Handke, M. Rings in the structure of silicate glasses. *J. Mol. Struct.* **1999**, *511–512*, 281–285. [CrossRef]
38. Keiffer, S.W. Thermodynamics and lattice vibrations of minerals: 2. Vibrational characteristics of silicates. *Rev. Geophys. Space Phys.* **1979**, *17*, 20–34. [CrossRef]

Disclaimer/Publisher's Note: The statements, opinions and data contained in all publications are solely those of the individual author(s) and contributor(s) and not of MDPI and/or the editor(s). MDPI and/or the editor(s) disclaim responsibility for any injury to people or property resulting from any ideas, methods, instructions or products referred to in the content.